CONF-860421--58

CONTROL OF HELIUM EFFECTS IN IRRADIATED MATERIALS BASED ON THEORY AND EXPERIMENT*

L. K. Mansur, E. H. Lee, P. J. Maziasz, and A. F. Rowcliffe

Metals and Ceramics Division
Oak Ridge National Laboratory
Oak Ridge, TN 37831 (USA)

CONF-860421--58

DE86 013275

ABSTRACT

Helium produced in materials by (n,α) transmutation reactions during neutron irradiations or subjected in ion bombardment experiments causes substantial changes in the response to displacement damage. In particular, swelling, phase transformations and embrittlement are strongly affected. Present understanding of the mechanisms underlying these effects is reviewed.

Key theoretical relationships describing helium effects on swelling and helium diffusion are described. Experimental data in the areas of helium effects on swelling and precipitation is reviewed with emphasis on critical experiments that have been designed and evaluated in conjunction with theory. Confirmed principles for alloy design to control irradiation performance are described.

---

*Research sponsored by the Division of Materials Sciences and Office of Fusion Energy, U.S. Department of Energy, under contract DE-AC05-840R21400 with Martin Marietta Energy Systems, Inc.

DISCLAIMER

1. INTRODUCTION

Helium will accumulate at high rates in structural materials for fusion reactors because of neutron-induced transmutation reactions. The high potency of helium for altering irradiation-induced microstructures has been confirmed by extensive research. Through theory and experiments that focus on mechanisms, it has been shown that helium is a main determining factor in swelling [1]. Similarly, high temperature embrittlement is widely understood to be associated with helium-filled cavities at grain boundaries [2]. It has been learned also that helium may produce significant changes in radiation-induced phase stability [3].

In the present paper the theory describing the onset of swelling and its dependence on helium is outlined. Critical experiments designed to probe mechanisms are highlighted. The understanding created by this combined theoretical and experimental approach has led to a powerful prescription for the design of swelling resistant alloys. Principles for the control of helium embrittlement follow analogous lines. Some observations of the strong effects of helium on precipitation are described together with possible mechanisms underlying these phenomena.

2. CAVITY CRITICAL RADIUS AND CRITICAL NUMBER OF GAS ATOMS

2.1 Origins

Various aspects of the critical quantities for swelling have been discussed by a number of authors [4-12]. Critical quantities arise as roots to the equation

$$\frac{dr_c}{dt} = \frac{\Omega}{r_c}[Z_v^c D_v C_v - Z_i^c D_i C_i - Z_v^c D_v C_v^e(r_c)] \qquad (1)$$

Here r_c denotes cavity radius, t time, and Ω atomic volume. The symbol Z^c denotes capture efficiency of a cavity for point defects, and $D = D^o \exp(-E^m/kT)$ is the point defect diffusion coefficient, where D^o is a constant, E^m is the point defect migration energy and kT has its usual meaning. Total point defect concentrations are denoted by C in physical units, while the thermal equilibrium concentration at a cavity is $C^e(r_c)$. These quantities are specialized by subscripts v or i for vacancies and interstitials. The concentrations C depend on irradiation variables and materials properties such as dose rate, temperature, microstructural sink densities and point defect properties. Full expressions are given elsewhere [1]. The thermal equilibrium vacancy concentration is

$$C_v^e(r_c) = C_v^o \exp[-(P_g - \frac{2\gamma}{r_c}) \frac{\Omega}{kT}] , \qquad (2)$$

where C_v^o is the bulk thermal equilibrium vacancy concentration, P_g is gas pressure and γ is the surface free energy.

An analytical approach to obtaining the roots of Eq. (1) is described in Ref. [1]. Exact mathematical solutions are possible where the gas pressure is related to the number of gas atoms in a cavity either through the ideal or the Van der Waals gas laws. It is also possible to retain the exact Van der Waals solution form for the case of very high pressure, where a more complex gas law must be used, as is described subsequently. Relevant relationships concerning the critical quantities are given below. These represent a generalization of relationships published earlier [1].

2.2 Relationships Among Critical Quantities

Figure 1 gives the form of results generated by Eq. (1). The positions of the curves relative to the axis depend strongly on temperature, dose rate, sink strength and other properties, while the general features do not. For the smaller number of contained gas atoms, n_g^1 indicated in the figure, there are two physical roots $r_c^s(n_g)$ and $r_c^c(n_g)$. The superscripts denote stable and critical cavity radii, respectively. A cavity with n_g^1 gas atoms tends to remain at r_c^s. If fluctuations in point defect absorption bring the cavity above the corresponding r_c^c it will grow inexorably, driven by the dislocation-cavity bias [13]. If the cavity has no gas, its critical radius is the largest possible, r_c^o, and the corresponding r_c^s is zero. Unless the gap $r_c^c - r_c^s$ is small in terms of number of vacancies, however, nucleation of growing cavities by fluctuations is unlikely [14].

For a larger number of gas atoms, a situation that could arise by the continuing absorption of helium, r_c^s and r_c^c approach each other. For a critical number of gas atoms n_g^*, r_c^s and r_c^c coincide at what we term the minimum critical radius, r_c^*. For more gas atoms, $n_g^3 > n_g^*$, there are no physical roots of Eq. (1) and a cavity of any size will grow continually. In cases of physical interest where r_c^* is a few nm, rapid swelling does not occur until cavities have accumulated n_g^* gas atoms (and therefore reached radius r_g^*).

Without gas the critical radius is given by

$$r_c^o = \frac{2\gamma}{f} , \qquad (3)$$

where f is a generalized "stress" due to excess point defect absorption,

$$f = \frac{kT}{\Omega} \ln\left[\frac{Z_v^c D_v C_v - Z_i^c D_i C_i}{Z_v^c D_v C_v^o}\right] . \qquad (4)$$

The minimum critical radius is given by

$$r_c^* = r_c^o \left[\frac{1 + \delta}{2 + \delta}\right], \qquad (5)$$

where $\delta = (1 + 3\beta)^{1/2}$ and $\beta = Bf/kT$, where B is the Van der Waals volume exclusion coefficient. (Equations (5–7) here are obtained as an equivalent rearrangement [15] of Eqs. (30–32) of Ref. [1].) The critical number of gas atoms is

$$n_g^* = \frac{32\pi\gamma^3}{f^2 kT} \frac{(1 + \delta)^2}{(2 + \delta)^4} , \qquad (6)$$

or

$$n_g^* = \frac{8\pi\gamma r_c^{o2}}{kT} \frac{(1 + \delta)^2}{(2 + \delta)^4} . \qquad (7)$$

This analysis also applies to cavities in a material under applied stress σ. For cavities in grain boundaries f is replaced with σ_t, the applied stress normal to the grain boundary. For cavities in a grain interior f is replaced with σ_h, the hydrostatic tensile stress [8]. Helium embrittlement at elevated temperatures is thus analyzed with a mathematically analogous treatment.

Substituting Eqs. (5) and (7) into the modified Van der Waals gas law

$$P_g = n_g kT/(\tfrac{4}{3}\pi r_c^3 - n_g B) , \qquad (8)$$

gives the gas pressure at the point where the cavity begins bias driven growth. This pressure (or number of gas atoms) is related but not equal to the equilibrium gas pressure (or number of gas atoms). The result is

$$\frac{P_g^*(r_c^*)}{P_g^{eq}(r_c^*)} = \frac{1}{2+\delta} \Big/ \left(\frac{2+\delta}{3} - \frac{B}{\Omega}\frac{\ell n\, S}{1+\delta}\right) , \tag{9}$$

where S denotes the enclosed argument in Eq. (4). Since $\delta \gg 1$ a cavity at r_c^* about to begin bias driven growth is considerably underpressurized with respect to an equilibrium bubble.

In the ideal gas limit ($B \to 0$) or $(B/\Omega)\ell n\, S \ll 1$), the above results reduce to

$$r_c^* = \frac{2}{3} r_c^o \tag{10}$$

and

$$n_g^* = \frac{128\pi\gamma^3\Omega^2}{81(kT)^3(\ell nS)^2} \tag{11}$$

or

$$n_g^* = \frac{32\pi\gamma r_c^{o2}}{81kT} . \tag{12}$$

The pressurization result is

$$\frac{P_g^*(r_c^*)}{P_g^{eq}(r_c^*)} = \frac{1}{3} , \tag{13}$$

or equivalently

$$\frac{n_g^*(r_c^*)}{n_g^{eq}(r_c^*)} = \frac{1}{3} \quad , \tag{14}$$

where n_g^{eq} is the number of gas atoms for a cavity in thermal equilibrium at r_c^*. Thus, if irradiation is discontinued, a cavity containing n_g^* gas atoms will tend to shrink to its thermal equilibrium radius for that number,

$$r_c^{eq} = r_c^* / \sqrt{3} \ . \tag{15}$$

2.3 Application at High Gas Densities

The forms of the exact solutions for the Van der Waals gas law, Eqs. (5–9), can be preserved for very high gas densities. A more complex equation of state than Eq. (8) is used to describe the relationship between number of gas atoms and pressure. The approach is to re-interpret the Van der Waals coefficient B as an effective coefficient, B^{ef}. Its value is determined by requiring consistency between the compressibility factor, $P_g V/n_g kT$, given by both gas laws. This work is described in Ref. [16]. The gas law formulated by Trinkaus [8] to span densities from those of solid to dilute gaseous helium, and which is in reasonable agreement with the forms proposed by Glasgow and Wolfer [17] is used. This approach gives analytical results for B^{ef}, which are then used in Eqs. (5–9).

Our results are shown in Fig. 2. Taking the atomic volume for materials of interest as $\sim 10^{-29}$ m^3, part (a) shows results for one helium atom in ten vacant sites and part (b) shows results for one helium atom in two vacant sites. The parameter v is the volume per helium atom. The dashed line plots the temperature-dependent but pressure independent

value of the Van der Waals exclusion volume, B [18]. The solid lines show the effective coefficient B^{ef}. It can be seen that the Van der Waals gas law is accurate over the entire temperature range for a density of one helium atom in ten vacancies but is inadequate for one helium atom in two vacancies. We find that B^{ef} departs significantly from B at about one helium atom per five vacancies. At this and higher densities, therefore, the effective volume exclusion coefficient should first be computed according to the analysis outlined above [16] and then used in Eqs. (5-9). As a practical matter, however, densities as high as this are not usually relevant at the critical radii of interest for the onset of swelling (typically several nanometers).

2.4 Bimodal Cavity Size Distributions

A very important result relating the above theory to the interpretation of experiments is the prediction of the development of a bimodal cavity size distribution. Measurement of such distributions can provide a direct measure of the critical radius r_c^*, and therefore, indirectly, a measure of n_g^*. The bimodal distribution contains a distinct class of stable cavities at radii less than r_c^*, typically several nanometers, and another class of growing cavities spread about much larger sizes. The formation of bimodal distributions in irradiation experiments where helium is present can be understood by reference to Fig. 1. As mentioned above, cavities containing less than n_g^* gas atoms reside at stable sizes $r_c^s < r_c^*$. Cavities containing more than this critical number grow continually by excess vacancy absorption. A separation of the two peaks in the measured distribution is thus expected to be marked by r_c^*.

A quantitative tool is therefore available that offers the following possibilities:

1. The variables on which critical radius (and critical number of gas atoms) depends functionally can be evaluated by applying the theory to the measured values.

2. Comparisons of the magnitudes of the critical quantities in different materials can reveal intrinsic differences in swelling propensity.

3. The basis for swelling resistance can be associated with a single measurable feature, r_c^*, even though this quantity is itself the net result of numerous dependencies on materials properties and irradiation conditions.

Cavity size distributions of this type are often observed. Table 1 lists numerous cases where bimodal distributions have been reported. They cover both ion and neutron irradiations and apply to a variety of alloy systems. It is interesting to note that most of the observations of bimodals have been made relatively recently, where improved equipment and techniques of electron microscopy have made possible the resolution of cavities as small as one nanometer in diameter.

All observations listed are for experiments where helium is present. This is consistent with our analysis above that predicts bimodal distributions, i.e. $r_c^* > 0$, only as a result of cavity pressurization. These results are taken as a confirmation of the general predictions of theory over a wide variety of conditions.

3. CONTROL OF SWELLING

3.1 Critical Radius Experiments

Most of the observations listed in Table 1 were made incidentally to the overall characterization of swelling and microstructure. It is also

possible to design experiments to induce a bimodal distribution for special purposes. Using the latter approach, we have recently investigated mechanisms of swelling variation with composition and principles for swelling resistant alloy design.

As one example, experiments to examine the low swelling behavior of the ferritic alloy Fe-10Cr have been carried out [55]. The critical radius was measured and the overall microstructure characterized. Based on these measurements more basic parameters of the material were extracted by mathematical analysis. It was concluded that the low swelling resulted from both a low dislocation bias for point defects and a very large imbalance in the sink strengths of cavities and dislocations due to a low dislocation density.

Another study [38] examined the basis of the extreme difference in swelling resistance between the pure ternary austenitic alloys Fe-15Ni-15Cr and Fe-35Ni-15Cr. This work helped solve the long-standing and important question of how the Ni content influences swelling. It was shown in ion irradiation studies by Johnston et al. [61] and subsequently by others also in neutron [62] and electron irradiations [63] that higher nickel content leads to lower swelling. It was found that much of the decrease in swelling was accounted for by an increase in the time (dose) to the onset of swelling.

Guided by the theory described in Section 2 above we suggested the hypothesis that this increase in dose could be due to an increase in the critical radius and critical number of gas atoms required for swelling.

Experiments were designed to test the idea. The key experiment was a sequenced helium injection, anneal, and irradiation. The injection and anneal step (400 appm, 675°C) produced similar bubble size distributions in the 15 and 35Ni alloys. The idea was to span the critical radii/critical number of gas atoms in each alloy. The subsequent irradiation would then be expected to cause the cavity size distributions to split into bimodals. The upper cutoff radius of the smaller size group would give a measure of r_c^* for each alloy.

Figure 3 shows the measured cavity size distributions after the irradiation to 40 dpa. Although the bubble distributions after the injection and anneal were reasonably similar, they are much different after the irradiation. In the low nickel alloy, no small cavities are present and the distribution is unimodal at a density of 5.3×10^{20} m^{-3}. In the high nickel alloy, the initial stable cavity density of 4.8×10^{21} m^{-3} decreased to 1.0×10^{21} m^{-3}, while the density of large cavities became nearly identical to that in the low nickel alloy, thus giving a bimodal. In the high nickel alloy, r_c^* was about 5 nm, while in the low nickel alloy it was concluded that r_c^* was below the electron microscope resolution limit, about 1 nm.

We interpret these results to show that the critical radii in the two alloys differs by a factor of 5 or more. Thus, the critical numbers of gas atoms must differ by at least a factor of 25 [Eq. (7)]. Such a large difference is consistent with the observed factor of difference in dose to begin swelling in irradiations where helium is accumulated concurrently

with dose. Further study of the microstructures and analysis using the theoretical expressions led to the conclusion that the bias of dislocation loops for excess interstitial absorption in the two alloys is much different and is the likely cause of the large difference in critical quantities. The underlying cause of the difference in bias of the two alloys is currently under investigation.

Other experiments show that two alloys where the critical quantities are similar can be made to exhibit very large differences in the dose to the onset of swelling [64]. Here the idea is to slow by microstructural refinement through compositional manipulation the accumulation rate of helium in each cavity, rather than to increase the critical number of gas atoms required for swelling. The slowing of the helium accumulation rate translates into a delay in the onset of swelling. Five simple alloys were irradiated simultaneously with self-ions and helium. One was the alloy Fe-15Cr-13Cr, another had 0.05% P added, while three others had the same amount of P together with additions of 0.8% Si or 0.2% Ti or both. Rapid swelling occurred in the ternary and the ternary with P. In the others, swelling was suppressed to relatively high doses.

The swelling suppression was correlated with the appearance of high densities of fine needle shaped Fe_2P precipitates. Maximum suppression occurred in the alloy with P, Si, and Ti, where the interfacial area of the phosphides was greatest. High resolution electron microscopy, Fig. 4, revealed profuse formation of helium bubbles on the interfaces. An analysis of these results based on the theory confirmed in quantitative terms that the swelling resistance imparted by phosphorous additions takes place

by a mechanism of helium dilution. By increasing the number of stable cavities collecting helium, the individual accumulation rate is lowered. Hence, for a given required critical number, the onset of swelling is delayed. Moreover, increasing the number of sinks also raises the critical radius. Very recent results show that swelling can be suppressed to doses of over 100 dpa and to helium levels of over several thousand appm in alloys of this type.

3.2 Alloy Design for Swelling Resistance

The foregoing discussion of theory and experimental results suggests clear principles for alloy design for swelling resistance:

1. By exploiting compositional and sink strength dependencies, increase the required critical number of gas atoms for the onset of swelling.

2. By introducing profuse traps for helium such as precipitate matrix interfaces by compositional and other means, such as thermomechanical treatment, increase the number of cavities and correspondingly slow the accumulation rate of helium in each cavity. This will increase the dose to the onset of swelling.†

3. Reduce the residual gas content of the alloy, so that the possibility of pre-existing gas triggering swelling by supplying the critical number of gas atoms is eliminated. This can be accomplished by alloying with gas gettering elements and by fabrication procedures.

---

†Note that this is not necessarily equivalent to maximizing pre-existing precipitates, since these may be unstable during irradiation. The precipitates should be optimized for formation and stability during the irradiation.

4.0 HELIUM DIFFUSION

The helium generation and diffusion rates dictate helium buildup in cavities and thus affect swelling and grain boundary embrittlement. Two general modes of diffusion of helium are visualized, substitutional diffusion via a vacancy mechanism and dissociative diffusion via an interstitial mechanism [65,66]. The former is the usual mechanism for substitutional diffusion, while the latter is akin to the anomalous fast diffusion phenomenon in lead, for example [67]. In the present discussion we do not consider helium bubble migration which may also contribute.

A subcase of the former is that where the neighboring vacancy necessary for a diffusion jump becomes bound to the helium-containing vacancy, and this complex diffuses like a divacancy. On the other hand the dissociative mechanism operates by retaining the helium for a time at an immobile trap; when the helium is released it diffuses rapidly as an interstitial before it is again trapped. There are several distinct physical mechanisms that may release the bound helium [68]. These include: thermal release, where the event is activated spontaneously by vibrational energy; recombination, where a self-interstitial annihilates the trapping vacancy; and direct displacement, where the helium atom is dislodged as a direct result of irradiation.

All these possibilities can be combined in a mathematical analysis that expresses the effective helium diffusion coefficient as a weighted composite. This is an adaptation of the approach developed for the effective diffusion coefficients of point defects undergoing trapping reactions [69]. The diffusion coefficient obtained when only the dissociative mode is

active was described previously [68]. The slightly generalized result that includes all the mechanisms discussed above is

$$D_{He}^{ef} = \frac{D_{He} + D_s \left[\frac{\kappa_{He} C_v \tau_s}{1 + G\Omega\tau_s + R_r C_i \tau_s + K_s \tau_s} \right]}{1 + \left[\frac{\kappa_{He} C_v \tau_s}{1 + G\Omega\tau_s + R_r C_i \tau_s + K_s \tau_s} \right]}, \qquad (16)$$

which arises directly from the definition

$$D_{He}^{ef}(C_{He} + C_s) = D_{He} C_{He} + D_s C_s \qquad (17)$$

and the rate equations for the helium concentrations in interstitial sites, C_{He}, and in substitutional sites, C_s, given previously [68]. The interstitial helium diffusion coefficient is given by $D_{He} = D_{He}^o \exp(-E_{He}^m/kT)$, where D_{He}^o is a constant and E_{He}^m is the interstitial helium migration energy. The coefficient for substitutional diffusion is given by $D_s = D_s^o \exp(-E_s^m/kT)$, where D_s^o is a constant. If the normal substitutional mechanism prevails, the activation energy of migration is $E_s = E_v^f + E_v^m$, where E_v^f is the vacancy formation energy. If the complex diffuses as if it were a divacancy with no perturbation produced by the inclusion of helium in the complex, the energy would be $E_s = E_v^f + E_{2v}^m - E_{2v}^b$, where E_{2v}^m and E_{2v}^b are the divacancy migration and binding energies.

In Eq. (16) $\kappa_{He} = 4\pi r_{Hev}(D_H + D_v)$ is the capture coefficient of a vacancy for interstitial helium, where r_{Hev} is the radius of the capture

volume. Similarly, $\tau_s = \upsilon_s \exp[(E^b_{Hev} + E^m_{He})/kT]$ is the mean residence time of He in a vacancy before it is released thermally as an interstitial, where υ_s is the attempt frequency and $E^b_{H\ v}$ is the binding energy of a helium atom to a vacancy. The generation rate of interstitial helium by direct displacement of trapped helium is given by G', per unit volume per unit time per unit fractional concentration of substitutional helium ($C_s\Omega$). The symbol $R_r = 4\pi r_r D_i$ is the coefficient of replacement, where the self-interstitial dislodges the substitutional helium, and r_r is the radius of the replacement volume.

Equation (16) allows side-by-side comparisons of the relative importance of each physical mechanism. Comparing the term in D_{He} to the term in D_s shows whether the dissociative mode or the substitutional mode dominates helium diffusion. Comparing the terms in the denominators in brackets shows which of the dissociative modes is most important in determining the trapped helium concentration. Thus, unity represents the thermal release mechanism, $G'\Omega\tau_s$ represents direct displacement of the helium, $R_r C_i \tau_s$ represents the self-interstitial replacing the helium, and $K_s\tau_s$ represents loss of the complex to sinks. By the methods given in Ref. [69] and in Section 3 of Ref. [68], the effective migration energies are easily obtained. The effective migration energies for the various possible dominant mechanisms are shown in Table 2. Figure 5 is a map in the space of temperature and dose rate showing regimes of dominance among the dissociative mechanisms for pure nickel. Generally, when thermal release dominates the dissociative mode, it is only necessary to compare the numerical value of $E^b_{Hev} + E^m_{He} - E^f_v$ to $E^m_v + E^f_v$ (or $E^f_v + E^m_{2v} - E^b_{2v}$).

Recent thermal desorption experiments at high temperatures for aluminum, silver, and gold favor the substitutional mode [66]. For nickel, however, similar experiments favor the dissociative mode with an energy consistent with the thermal release mechanism [70]. However, very recent results by nuclear scattering, a method that measures the diffusion profile of helium remaining in the material rather than that helium escaping through the surface, favor the substitutional mode or possibly bubble migration mode for Ni [71]. A second difference between the two types of experiments is that the specimens in the nuclear scattering experiments may retain a larger amount of displacement damage caused by the energetic helium injection, so that trapping at extended defects is possible.

Figure 6 shows recent results obtained [71] for several metals using the nuclear interaction technique based on the reaction $d(^3He,p)^4He$. At the temperatures indicated on the figure, it was found in nickel that the helium remained essentially where it was implanted. For iron the helium showed some migration from the implanted region and part of it collected near the specimen surface. In the case of zirconium no detectable helium remained in the implanted region; much of it appears to have migrated to and become trapped near the surface. These results may suggest a possible link to the analysis surrounding the critical number of gas atoms in Sections 2 and 3. Zirconium appears to be extremely radiation damage resistant; it is not known to exhibit swelling or irradiation embrittlement [72]. It is possible that the rapid diffusion of helium in zirconium may be the reason that it does not agglomerate to form traps. In particular, if a cavity cannot build up the critical number of gas atoms in this

material then the theory shows that swelling and helium embrittlement will not occur. On the other hand, nickel is highly swelling prone, and it is consistent that the measured helium mobility in this metal is very low.

5. HELIUM AND PHASE INSTABILITY

Much of the work on radiation induced phase instability (RIP) began recently. It took time for RIP to be appreciated as a pervasive phenomenon, awaiting both the advent of analytical electron microscopy and a gradual movement away from preoccupation with only cavity and dislocation microstructure. With respect to helium it was widely anticipated that the gas should have little effect on precipitation since it is chemically inert. However, it was shown subsequently that helium causes extreme changes in radiation affected precipitation. Some observed effects include suppression of radiation-induced precipitation, alterations in the sequence of phase transformations and changes in the mixture of types as well as changes in the composition of phases. Most of the work done in this area has been in the Fe-Ni-Cr alloy system, and the examples cited below reflect this.

The first example covers Ni-ion irradiations of Ti-modified type 316 stainless steel at 625°C [73]. In Fig. 7 the results of two types of experiments are shown for comparison, both at an irradiation dose of 70 dpa. On the left is the microstructure of a specimen irradiated simultaneously with 4 MeV Ni ions and 200–400 keV He ions at a rate of 0.2 appm/dpa. On the right is the result for helium preinjected to the

same level followed by a nickel ion irradiation to the same dose. The differences are remarkable. In the simultaneous case, G-phase particles form profusely. There is also significant swelling, represented by the large cavities that are generally attached to the particles. In the preinjected case G-phase precipitation is suppressed. Small gas filled cavities are observed, however (insert). They are interpreted as the stable cavities of the analysis of Section 3. The mode of helium injection is responsible for the drastic difference.

A neutron experiment was also carried out with and without preinjected helium in a solution annealed type 316 stainless steel. The helium injection of 110 appm was achieved using a cyclotron and the subsequent irradiation was carried out in the EBR-II reactor [74]. Figure 8 shows the microstructural results observed at 8.4 dpa. The top micrographs are for specimens irradiated at 500°C. Those at the bottom show corresponding results at 625°C. The right micrographs are for specimens that were preinjected, while those on the left were not. The entire microstructure is altered by the helium preinjection. The aspects of main interest here are that the volume fraction of precipitates and the distribution of types are radically altered by the preinjected helium. Figure 9 shows the results in the form of pie charts, where overall circular areas indicate relative volume fractions at each helium and temperature condition and the segment angles indicate the fraction of major phase types. At the high temperature, helium promotes formation of Laves phase, which is a thermally stable phase that also forms on aging. The phosphide and η phases on the other hand are radiation enhanced. At the lower temperature, helium suppresses precipitation entirely.

The last example is a Ni-ion experiment on a Ti-modified type 316, with and without simultaneous helium injection at a rate of 20 appm/dpa. Figure 10 shows results [75]. On the left are the results for Ni-ions only and on the right are those for the simultaneous irradiation. While the precipitation does not appear to show as marked a difference as above with pre-injected helium, there are important differences in the phases. With no helium the precipitates are mainly G-phase, a true radiation induced nickel-rich silicide that contains about 50 at. % Ni and 30 at. % Si [76], while the matrix contains only 15 at. % Ni and 2 at. % Si. With He, however, precipitates are mainly n-phase, a phase moderately enriched in Ni (30 at. %) and Si (16 at. %), a phase that does occur thermally to a much lower extent.

An explanation for these results invokes a fixed number of solute atoms being distributed over a larger number of segregation sites when helium is present [1]. When irradiation begins, interstitial loops nucleate profusely. If helium is present, the vacancies corresponding to the interstitials are trapped by the gas. Thus both more loops and vacancy clusters survive when helium is available. Otherwise, the vacancies eventually annihilate most of the interstitials that rapidly clustered initially to form the loops. The vacancy clusters give rise to a fine distribution of cavities. Thus, both dislocation loops and cavities are increased by helium [1,3].

Both the cavities and loops are sites for solute segregation. Radiation-induced and enhanced phases depend on solute segregation, particularly Ni and Si, for their formation. Since the number of solute atoms is fixed, the larger number of sinks in the helium-containing case

leads to a dilution of the solute buildup at each sink. Radiation-induced precipitates are thus suppressed. However, precipitation of the normally encountered thermal phases is less affected although there may be some effects by precipitation site modification; the elements required are less driven by solute segregation to be dispersed at many sites and are thus available for incorporation into thermal precipitates.

Changes in precipitation are important both to dimensional stability and mechanical properties. We have shown previously that cavities attached to precipitates grow more rapidly than those in the matrix. This occurs by the recently recognized mechanism of point defect collection and short-circuit diffusion at the precipitate-matrix interface [77,78]. A relatively few large precipitates increase swelling, while a profuse distribution of fine precipitates both exhibits minimal collector effect because of their small size and delays the achievement of the critical number of gas atoms by helium dilution. Similar considerations apply for helium embrittlement, where helium dispersion should reduce its prevalence at grain boundaries.

Precipitation during irradiation may also cause hardening or softening, affecting tensile and creep properties. Hardening may occur by precipitate pinning of dislocations, while softening may occur by depletion of the matrix of solid solution strengtheners or by coarsening of precipitates. Since helium can affect precipitation so strongly this becomes a major consideration; more research is obviously needed on the connections between helium, phase instability and properties.

6. SUMMARY AND DISCUSSION

Two additional areas concerning helium behavior in materials require further substantial research efforts. 1. The study of helium diffusion characteristics is an extremely important area. Recent evidence suggests a correlation between helium diffusivity and propensity for swelling and helium embrittlement. 2. Helium has been found to exert very strong effects on phase stability in austenitic Fe-Cr-Ni base alloys. Phase transformations can be suppressed entirely or the sequence of phase changes and the relative abundance of various phases can be altered. The precipitate dispersion and its interaction with other microstructural features in turn determines the changes in physical and mechanical properties of the alloy during irradiation. There is a strong need to understand and to be able to predict the interaction of helium and phase instability and the ultimate effect on properties.

A key result of theoretical and experimental research on helium is the concept of a critical cavity radius and critical number of gas atoms for rapid swelling. In cases of interest the onset of swelling is determined by the time to accumulate the critical number of gas atoms in cavities. The critical number of gas atoms is calculable from theory and depends on irradiation parameters such as temperature and dose rate and on materials properties such as bias, vacancy migration energy and microstructural sink densities. The minimum critical radius, which has a direct correspondence with the critical number of gas atoms, is measurable by electron microscopy when it is above the microscope resolution limit. Its existence in many

alloy systems over a wide range of irradiation conditions has been verified by numerous observations of bimodal cavity size distributions. Under given conditions the critical number of gas atoms represents a gauge of resistance to the onset of swelling in a single measurable quantity.

A twofold principle for alloy design for swelling resistance emerges from this analysis, as represented in Fig. 11. 1) Maximize the critical number of gas atoms required for rapid cavity growth and minimize the rate of gas accumulation in a cavity. By compositional variations and by increasing the microstructural sink density it has been found that critical radii can be increased at least several-fold, corresponding to up to about an order of magnitude in critical number of gas atoms. 2) Introduce elements that result in a very fine precipitate dispersion during irradiation. By this approach it is possible to increase the number of cavities by orders of magnitude. This has the result of slowing the helium accumulation rate in each cavity by dilution of the generated gas among more sites. By combining these two approaches, delays of swelling to more than 100 dpa and to several thousand appm helium have been demonstrated in otherwise very high swelling austenitic Fe-Cr-Ni base alloys. In principle, longer delays should be possible. In principle this approach applies equally to other alloy systems such as ferritic alloys or vanadium and copper base alloys under consideration as fusion reactor materials.

These principles apply directly also to pure helium embrittlement caused by gas bubbles on grain boundaries. The expressions for the critical quantities given by Eqs. (5) and (7) have exact mathematical analogs for embrittlement. In the case of swelling the driving stress is the excess vacancy condensation driven by point defect generation. In the case of embrittlement the driving force is the applied stress. To find the critical radius and critical number of gas atoms for grain boundary cavities the term f is simply replaced by σ_t, the tensile stress normal to the grain boundary. However, it should be noted that pure helium embrittlement described by such a picture probably only occurs at very high temperature. At lower temperatures the situation will be compounded by the contributions of radiation induced solute segregation to grain boundaries and by hardening of the matrix by radiation induced defects.

The previous discussion has emphasized delaying the onset of swelling. After swelling begins the growth kinetics of cavities also depend strongly on dose rate, temperature, bias and the ratio, Q, of sink strengths of dislocations to those of cavities, and to the ratios of the sink strengths of other sinks to those of cavities. For example, the swelling rate is low whenever either the cavities or dislocations are by far the dominant sink for point defects. When the system moves toward parity of dislocation and cavity sink strengths, the swelling rate becomes maximum. This analysis and its results are described in detail elsewhere [79].

REFERENCES

1. L. K. Mansur and W. A. Coghlan, J. Nucl. Mater. 119 (1983) 1.
2. H. Schroeder, W. Kesternich, and H. Ullmaier, Nucl. Eng. and Design/Fusion 2 (1985) 65.
3. K. Farrell, P. J. Maziasz, E. H. Lee, and L. K. Mansur, Rad. Eff. 78 (1983) 277.
4. G. R. Odette and S. C. Langley, Proc. Int. Conf. on Radiation Effects and Tritium Technology for Fusion Reactors (Oct. 1975), Gatlinburg, Tenn., CONF-750989, eds. J. S. Watson and F. W. Wiffen, p. I-395.
5. M. R. Hayns, M. H. Wood and R. Bullough, J. Nucl. Mater. 75 (1978) 241.
6. K. C. Russell, Acta Metall. 26 (1978) 1615.
7. R. E. Stoller and G. R. Odette, J. Nucl. Mater. 131 (1985) 118.
8. H. Trinkaus, Radiation Effects 78 (1983) 189.
9. W. A. Coghlan and L. K. Mansur, J. Nucl. Mater. 122 & 123 (1984) 495.
10. A. Hishinuma and L. K. Mansur, J. Nucl. Mater. 118 (1983) 91.
11. J. A. Spitznagel, W. J. Choyke, N. J. Doyle, R. B. Irwin, J. R. Townsend, and J. R. McGruer, J. Nucl. Mater. 108 & 109 (1982) 537.
12. R. Bullough and S. M. Murphy, J. Nucl. Mater. 133 & 134 (1985) 92.
13. A. D. Brailsford and R. Bullough, J. Nucl. Mater. 44 (1972) 121.
14. M. R. Hayns and L. K. Mansur, J. Nucl. Inst. & Meth. in Phys. Res. (in press).
15. H. Trinkaus and L. K. Mansur, unpublished work.
16. L. K. Mansur, to be submitted to J. Nucl. Mater.

17. B. B. Glasgow and W. G. Wolfer, Damage Analysis and Fundamental Studies Quarterly Progress Report, DOE/ER-0046/12 (1983).

18. N. V. Tsederberg, V. N. Popov and N. A. Morozova, Thermodynamic and Thermophysical Properties of Helium, Israel Program for Scientific Translations, Jerusalem, 1971, pp. 18–19.

19. H. R. Brager and J. L. Straalsund, J. Nucl. Mater. 46 (1973) 134.

20. P. J. Maziasz, F. W. Wiffen, and E. E. Bloom, pp. I-259 in Conf. Proc. Radiation Effects and Tritium Technology for Fusion Reactors, eds., J. S. Watson and F. W. Wiffen, USERDA, CONF-750989, Vol. 1 (1976).

21. P. J. Maziasz and M. L. Grossbeck, J. Nucl. Mater. 103 & 104 (1981) 987.

22. A. Hishinuma, J. M. Vitek, J. A. Horak, and E. E. Bloom, p. 92 in Proc. 11th ASTM Symposium on the Effects of Radiation on Materials, Scottsdale, AZ, June 1982, p. 92, H. R. Brager and J. S. Perrin, eds.

23. H. R. Brager and F. A. Garner, J. Nucl. Mater. 103 & 104 (1981).

24. H. R. Brager and F. A. Garner, J. Nucl. Mater. 108 & 109 (1982) 347.

25. H. R. Brager and F. A. Garner, J. Nucl. Mater. 117 (1983) 159–176.

26. H. R. Brager and F. A. Garner, p. 1 in Conf. Proc. on Dimensional Stability and Mechanical Behavior of Irradiated Metals and Alloys, British Nuclear Energy Society, London, England (1984).

27. P. J. Maziasz and D. N. Braski, J. Nucl. Mater. 122 & 123 (1984) 305.

28. D. Imeson, et al., J. Nucl. Mater. 122 & 123 (1984) 266.

29. J. A. Spitznagel, et al., in Ref. [11].

30. A. Kohyama, et al., J. Nucl. Mater. 117 (1983) 143.

31. A. Kohyama, G. Aryault, and N. Igata, J. Nucl. Mater. 122 & 123 (1984) 224.

32. A. Kohyama, et al., p. 277 as in Ref. [22].

33. R. L. Sindelar, G. L. Klucinski, and R. A. Dodd, J. Nucl. Mater. (1984) 246.

34. R. L. Sindelar, G. L. Kulcinski, and R. A. Dodd, J. Nucl. Mater. (1985) 544.

35. E. H. Lee, N. H. Packan, and L. K. Mansur, J. Nucl. Mater. 117 (1983) 123.

36. E. H. Lee, N. H. Packan, M. B. Lewis, and L. K. Mansur, Nucl. Inst. and Meth. (to be published).

37. V. Levy, D. Gilbon, and C. Rivera, p. 317 in Effects of Radiation on Materials: Twelfth International Symposium, ASTM-STP 870, eds. F. A. Garner and J. S. Perrin, Amer. Soc. for Testing and Materals (1985).

38. E. H. Lee and L. K. Mansur, Phil. Mag. A 52 (1985) 493.

39. D. J. Mazey and R. S. Nelson, p. I-240 in Conf. Proc. on Radiation Effects and Tritium Technology for Fusion Reactors, eds. J. S. Watson and F. W. Wiffen, USERDA, CONF-750989, Vol. 1 (1976).

40. N. H. Packan and K. Farrell, J. Nucl. Mater. 85 & 86 (1979) 677–681.

41. N. H. Packan and K. Farrell, Nuclear Technology 3 (1983) 392.

42. S. C. Agarwal, et al., J. Nucl. Mater. 85 & 86 (1979) 653.

43. E. A. Kenik, J. Nucl. Mater. 85 & 86 (1979) 659.

44. E. A. Kenik and E. H. Lee, p. 493 in Conf. Proc. on Phase Stabiity During Irradiation, eds., J. R. Holland, L. K. Mansur, and D. I. Potter, The Metallurgical Society of AIME, Warrendale, PA (1981).

45. W. J. Choyke, et al., J. Nucl. Mater. 85 & 86 (1979) 647.

46. S. Wood, et al., p. 455 in Effects of Radiation on Materials: Tenth Conference, ASTM-STP 725, American Society for Testing and Materials (1981).

47. G. Ayrault, H. A. Hoff, F. V. Nolfi, Jr., and A. P. L. Turner, J. Nucl. Mater. 103 & 104 (1981) 1035.

48. J. M. Vitek and R. L. Klueh, J. Nucl. Mater. 122 & 123 (1984) 254.

49. J. M. Vitek and R. L. Klueh, p. 551 in Proc. Topical Conf. on Ferritic Alloys for Use in Nuclear Energy Technologies, eds. J. W. Davis and D. J. Mickel, The Metallurgical Society of AIME (1984).

50. L. L. Horton, Ph.D. Thesis, Oak Ridge National Laboratory Report, ORNL/TM-8303 (1982).

51. L. L. Horton and J. Bentley, p. 259 in Proc. Topical Conf. on Ferritic Alloys for Use in Nuclear Energy Technologies, eds. J. W. Davis and D. J. Michel, The Metallurgical Society of AIME (1984).

52. L. L. Horton, J. Bentley, and W. A. Jesser, J. Nucl. Mater. 103 & 104 (1981) 1085.

53. K. Farrell and E. H. Lee, p. 383 in Effects of Radiation on Materials: Twelfth International Symposium, ASTM-STP 870, eds. F. A. Garner and J. S. Perrin, Amer. Soc. for Testing and Materials (1985).

54. K. Suzuki, et al., J. Nucl. Mater. 133 & 134 (1985) 632.

55. L. L. Horton and L. K. Mansur, p. 344 in Effects of Radiation on Materials: Twelfth International Symposium, ASTM-STP 870, eds. F. A. Garner and J. S. Perrin, Amer. Soc. for Testing and Materials (1985).

56. M. Tanaka, E. E. Bloom, and J. A. Horak, J. Nucl. Mater. 103 & 104 (1981) 895.

57. B. A. Loomis, B. J. Kestel, S. B. Gerber, and G. Ayrault, "Effect of Helium on Swelling and Microstructural Evolution in Ion-Irradiated V-15Cr-5Ti Alloy," Proc. Second Int. Conf. on Fusion Reactor Materials, April, 1986, to be published in J. Nucl. Mater.

58. B. A. Loomis and S. B. Gerber, J. Nucl. Mater. 103 & 104 (1981) 1193.

59. C. A. English, J. Nucl. Mater. 108 & 109 (1982) 104.

60. D. N. Braski, J. Nucl. Mater. 122 & 123 (1984) 676.

61. W. G. Johnston, J. H. Rosolowski, A. M. Turkalo, and T. Lauritzen, J. Nucl. Mater. 54 (1974) 24.

62. J. F. Bates and W. G. Johnston, p. 626 in Proc. AIME Conf. on Radiation Effects in Breeder Reactor Structural Materials, Scottsdale, AZ, ed. by M. L. Bleiberg and J. W. Bennett, The Metallurgical Society of AIME (1977).

63. A. Hishinuma, Y. Katano, and K. Shiraishi, J. Nucl. Mater. 103 & 104 (1981) 1063.

64. E. H. Lee and L. K. Mansur, this volume.

65. W. Schilling, p. 303 in Proc. of Yamada Conf. 5 on Point Defects and Defect Interactions in Metals, University of Tokyo Press, 1982.

66. V. Sciani and P. Jung, Rad. Effects 78 (1983) 87.

67. A. D. LeClaire, J. Nucl. Mater. 69 (1978) 70.

68. N. M. Ghoniem, S. Sharafat, J. M. Williams, and L. K. Mansur, J. Nucl. Mater. 117 (1983) 96.

69. L. K. Mansur, Acta Metall. 29 (1981) 375.

70. V. Philipps, K. Sonnenberg, and J. M. Williams, J. Nucl. Mater. 107 (1982) 271.

71. M. B. Lewis and K. Farrell, "Migration Behavior of Helium under Displacive Irradiation in Stainless Steel, Nickel, Iron, and Zirconium," Nucl. Inst. & Meth. (in press).

72. D. O. Northwood, Atomic Energy Review 154 (1977) 547.

73. E. A. Kenik and E. H. Lee, p. 493 in Proc. Conf. on Phase Stability During Irradiation, eds. J. R. Holland, L. K. Mansur, and D. I. Potter, The Metallurgical Society of AIME, 1981.

74. P. J. Maziasz, Ph.D. Thesis, Oak Ridge National Laboratory Report, ORNL-6121 (1984).

75. E. H. Lee, N. H. Packan, M. B. Lewis, and L. K. Mansur, J. Nucl. Inst. and Meth. (to be published).

76. E. H. Lee, P. J. Maziasz, and A. F. Rowcliffe, p. 191 in Proc. Conf. on Phase Stability During Irraidation, eds. J. R. Holland, L. K. Mansur, and D. I. Potter, The Metallurgical Society of AIME, 1981.

77. L. K. Mansur, Phil. Mag. A 44 (1981) 867.

78. E. H. Lee, A. F. Rowcliffe, and L. K. Mansur, J. Nucl. Mater. 103 & 104 (1981) 1475.

79. L. K. Mansur, Nuclear Technology 40 (1978) 5.

FIGURE CAPTIONS

Fig. 1. Calculated dependence of cavity growth rate on cavity size for the case of no contained gas for three different gas contents. The curve designated by n_g^* contains just the critical number of gas atoms and locates the minimum critical cavity radius, r_c^*.

Fig. 2. Calculation of the Van der Waals coefficient versus temperature for high as densities. Solid lines show the effective coefficient needed to keep the Van der Waals solutions accurate. Dashed lines show the reference pressure-independent result. In part a the gas density is approximately one helium atom per ten vacancies and in part b it is one helium atom per two vacancies.

Fig. 3. Cavity size distributions in low nickel (above) and high nickel (below) alloys after the helium injection-anneal-irradiation experiment described in the text. The helium content of 400 appm was injected at 75°C. The irradiation was done at the same temperature to a dose of 40 dpa.

Fig. 4. Low and high magnification micrographs of CW B12 alloy (Fe-13Cr-15Ni-0.8Si-0.2Ti-0.04C-0.05P) irradiated to 109 dpa/2000 appm He at 675°C.

Fig. 5. Mechanism map showing the regimes where thermal dissociation, complex-point defect recombination and direct displacement are calculated to dominate as a function of displacement rate and temperature for pure nickel.

Fig. 6. Concentration vs depth profiles for helium injected into iron, nickel and zirconium as determined by nuclear scattering using the $d(He^3,p)\alpha$ reaction [71].

Fig. 7. Results of irradiation of Ti-modified type 316 stainless steel to a dose of 70 dpa with nickel ions at 625°C. On the left is the microstructure for the case of simultaneous helium injection at 0.2 appm/dpa. On the right is the microstructure for the case where helium was preinjected to a level of 14 appm.

Fig. 8. Microstructures resulting from cyclotron preinjection of helium to 110 appm and irradiation in EBR-II reactor to a dose of 8.4 dpa. Irradiation temperature and presence or absence of helium are indicated on figure.

Fig. 9. Charts showing the relative volume fraction of precipitate (area of circles) and distributions of precipitate types (angle of segments) for the experiment shown in Fig. 8.

Fig. 10. Ti-modified stainless steel irradiated to 1, 40, and 70 dpa at 675°C with (right column) and without (left column) helium injection.

Fig. 11. Schematic illustration of recommended strategy for alloy design. Required critical number of gas atoms, n_g^*, is raised by alloying. At the same time the accumulation rate of gas atoms in a cavity is slowed by dilution on more cavities, which is accomplished by alloying to create a fine stable distribution of precipitates.

Table 1. Observations of bimodal cavity size distributions

Alloy	Irradiation	Investigators	References
Type 316 S.S.	Neutrons (EBR-II)	Brager & Straalsund (1973)	19
Type 316 S.S.	Neutrons (HFIR)	Maziasz & Coworkers (1976)	20
Type 316 S.S.	Neutrons (EBR-II)	Maziasz & Grossbeck (1981)	21
Type 316 S.S.	Neutrons (EBR-II)	Hishinuma & Coworkers (1982)	22
Type 316 S.S.	Neutrons (EBR-II)	Brager & Garner (1981,84)	23,24
Type 316 S.S.	Neutrons (HFIR)	Brager & Garner (1983,84)	25,26
Ti-Modified PCA	Neutrons (HFIR)	Maziasz & Braski (1984)	27
Ti-Modified PCA	Neutrons (HFIR)	Imeson & Coworkers (1984)	28
Type 304 S.S.	Ions (He Pre- or Coinjection)	Spitznagel & Coworkers (1982)	29
Type 316 S.S.	Ions (He Coinjection)	Kohyama & Coworkers (1983,84)	30,31,32
Austenitic Fe-Cr-Ni-Mo	Ions	Sindelar (1984)	33
Type 316 S.S.	Ions	Sindelar and Coworkers (1985)	34
Ti-Modified 316	Ions (He Coinjection, Pulsing)	Lee & Coworkers (1983,86)	35,36
Type 316 S.S. (Ti)	Ions (He Pre- or Coinjection)	Levy & Coworkers (1985)	37
Austenitic Fe-Cr-Ni	Ions (He Pre- or Coinjection)	Lee & Mansur (1985)	38
Type 321 S.S.	Ions (He Preinjection)	Mazey & Nelson (1976)	39
Austenitic Fe-Cr-Ni-Mo	Ions (He Pre- or Coinjection)	Packan & Farrell (1979,83)	40,41

Table 1 (Cont'd)

Alloy	Irradiation	Investigators	References
Austenitic Fe-Cr-Ni	Ions (He Coinjection)	Agarwal & Coworkers (1979)	42
Ti-Modified 316 S.S.	Ions (He Pre- or Coinjection)	Kenik & Coworkers (1979,81)	43,44
Type 304 S.S.	Ions (He Pre- or Coinjection)	Choyke & Coworkers (1978,81)	45
Type 316 S.S.	Ions (He Coinjection)	Wood & Coworkers (1981)	46
Type 316 S.S.	Ions (He Coinjection)	Ayrault & Coworkers (1981)	47
Ti-Modified 316	Ions (He Coinjection)	Hishinuma & Coworkers (1981)	22
9Cr-1MoVNb	Neutrons (HFIR)	Vitek & Klueh (1984)	48
12Cr-1MoVW	Neutrons (HFIR)	Vitek & Klueh (1984)	49
Fe-10Cr	Ions (He and H Coinjection)	Horton & Bentley (1981,84)	50,51,52
9Cr-1Mo	Ions (He Coinjection)	Farrell & Lee (1985)	53
HT-9 & HT-9 + 2% Ni	Ions (He Coinjection)	Suzuki & Coworkers (1985)	54
Fe-10Cr	Ions (He Preinjection)	Horton & Mansur (1985)	55
V-20Ti	Neutrons (EBR-II, He Preinjected)	Tanaka & Coworkers (1981) (Possible Incipient Bimodal)	56
V-15Cr-5Ti	Ions (He Coinjected)	Loomis & Coworkers (1986)	57
Nb	Ions (He Coinjected)	Loomis & Gerber (1981)	58
Cu	Neutrons (Pluto)	English (1982)	59
$(Ni_{0.78}Fe_{0.22})_3V$ LRO	Neutrons (HFIR)	Braski (1984)	60

Table 2. Effective helium migration energies

Mode	Mechanism	Energy
Dissociative	Thermal release	$E^b_{Hev} + E^m_{He} - E^f_v$
	Interstitial replacement	E^m_v
	Direct displacement	E^m_v (sink dominated)
		$E^m_v/2$ (recombination dominated)
Substitutional	Vacancy	$E^m_v + E^f_v$
	Divacancy	$E^f_v + E^m_{2v} - E^b_{2v}$

ORNL-DWG 85-15532

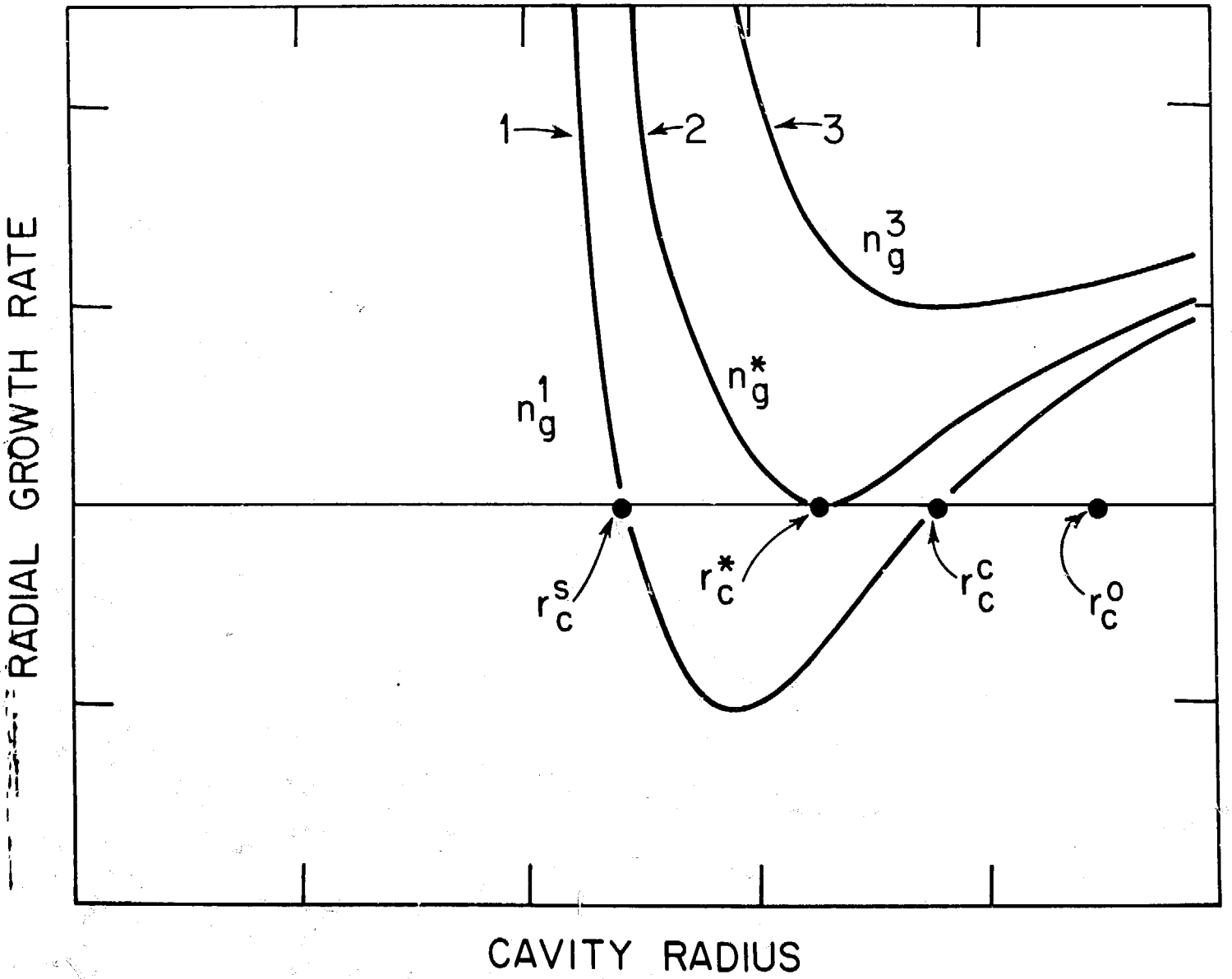

Fig 1. Mansur, et al

ORNL-DWG 86C-9101

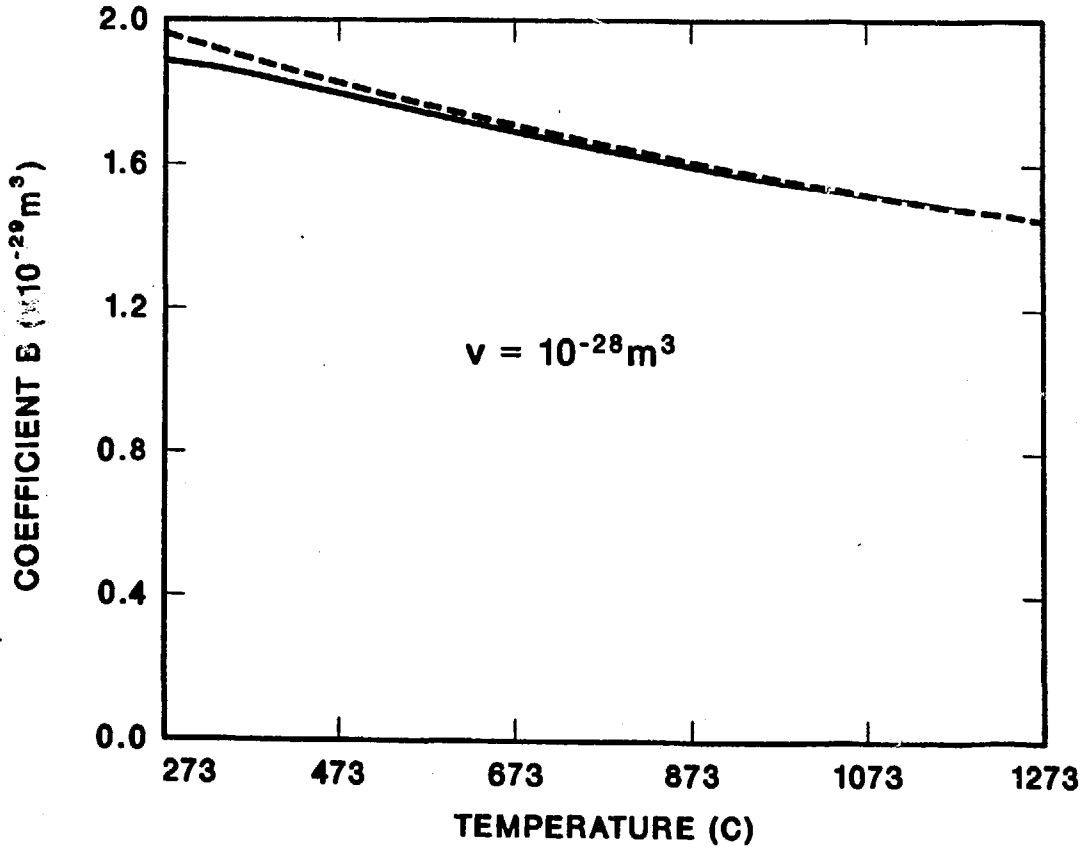

Fig 2a, Mansur, et al

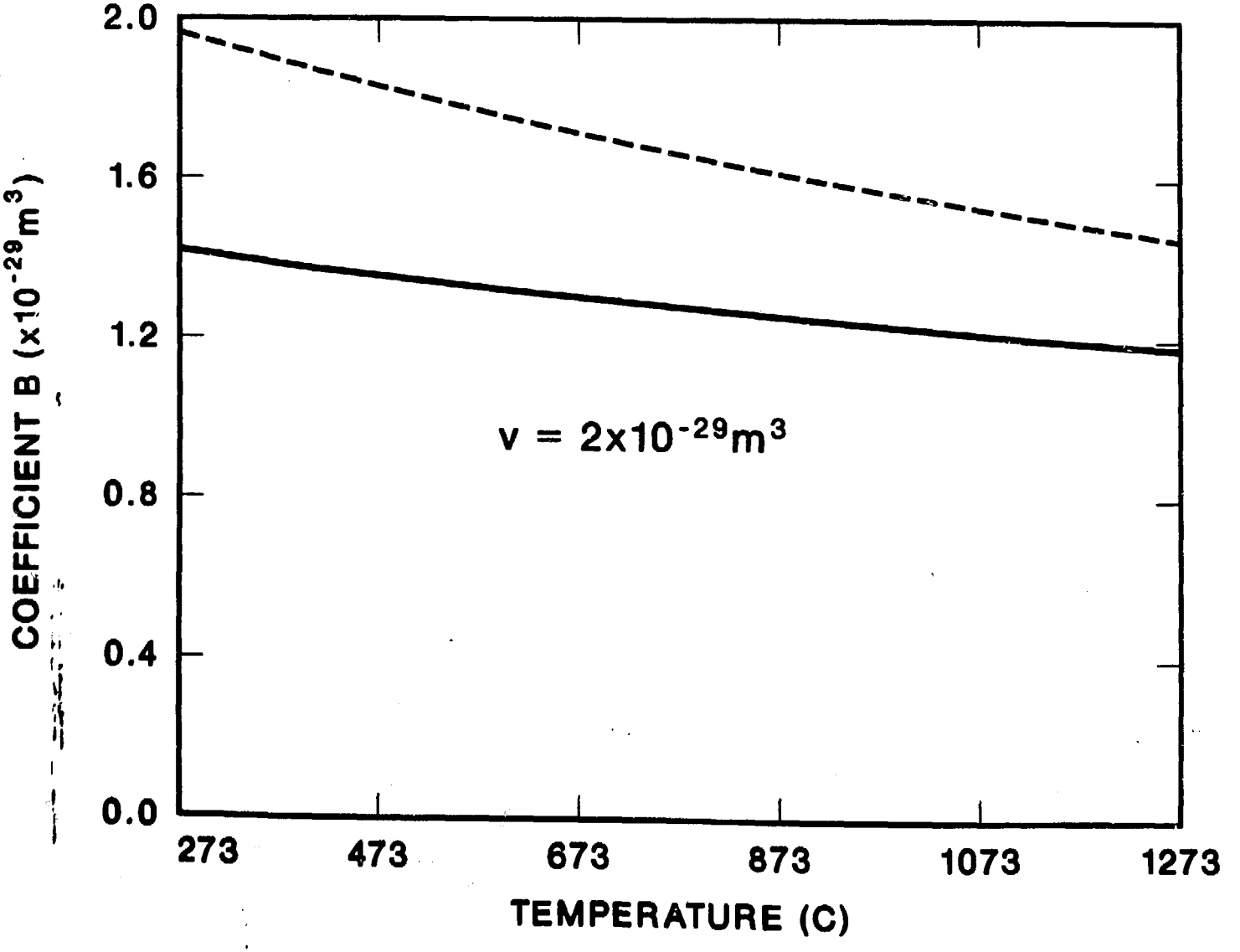

Fig 26, Mansur et al

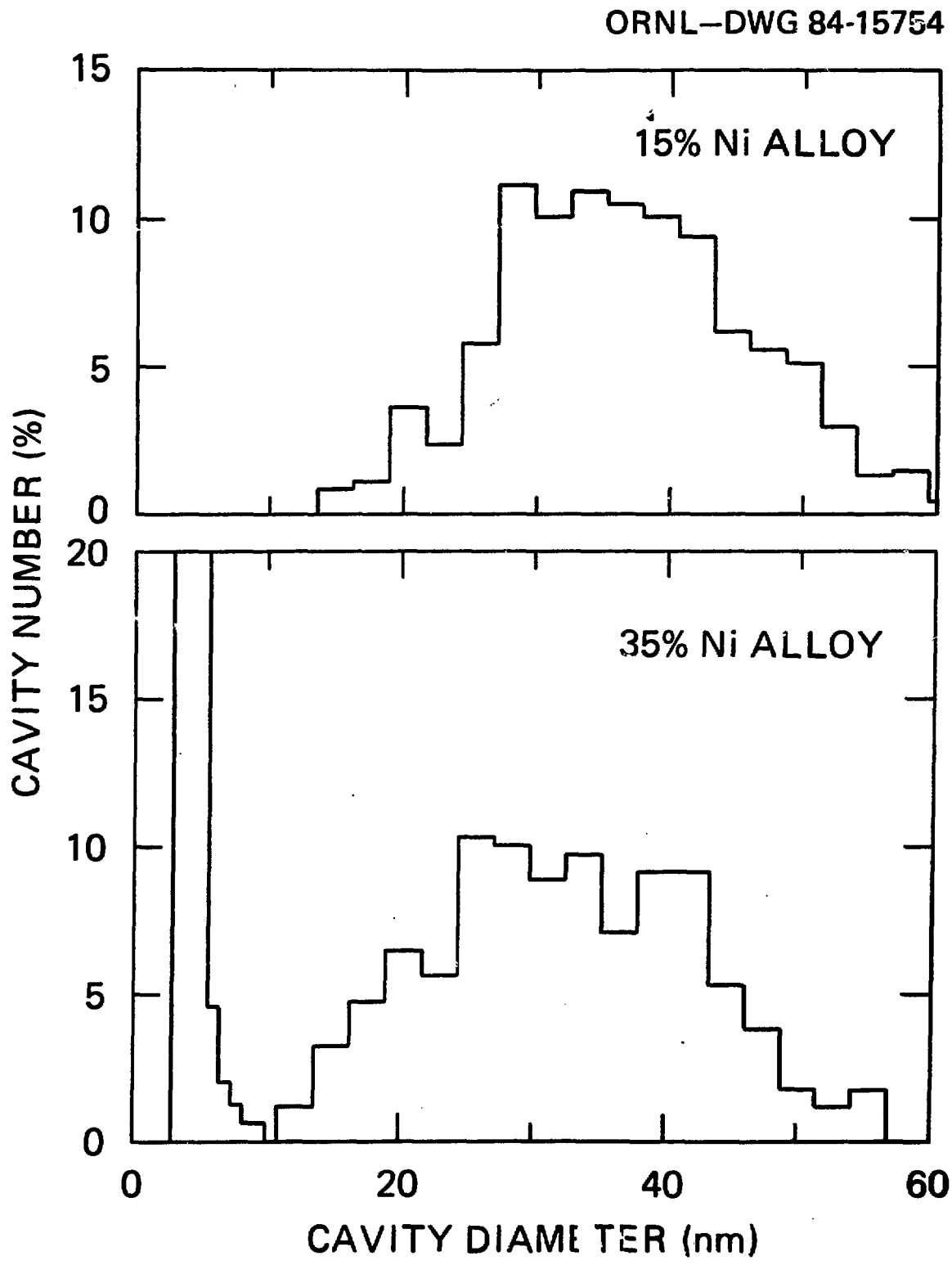

Fig 3, Mansur et al

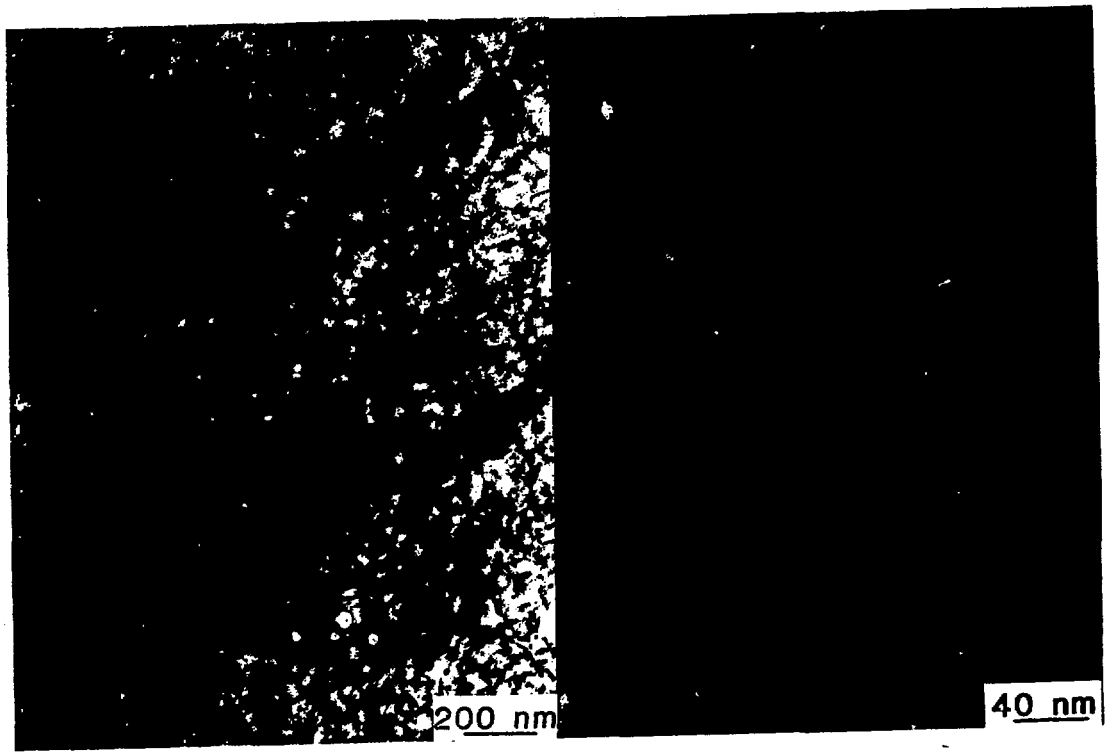

(Fe-13Cr-15Ni
-0.15Si-0.2Ti-
-0.05P)

Fig 4, Mansur et al

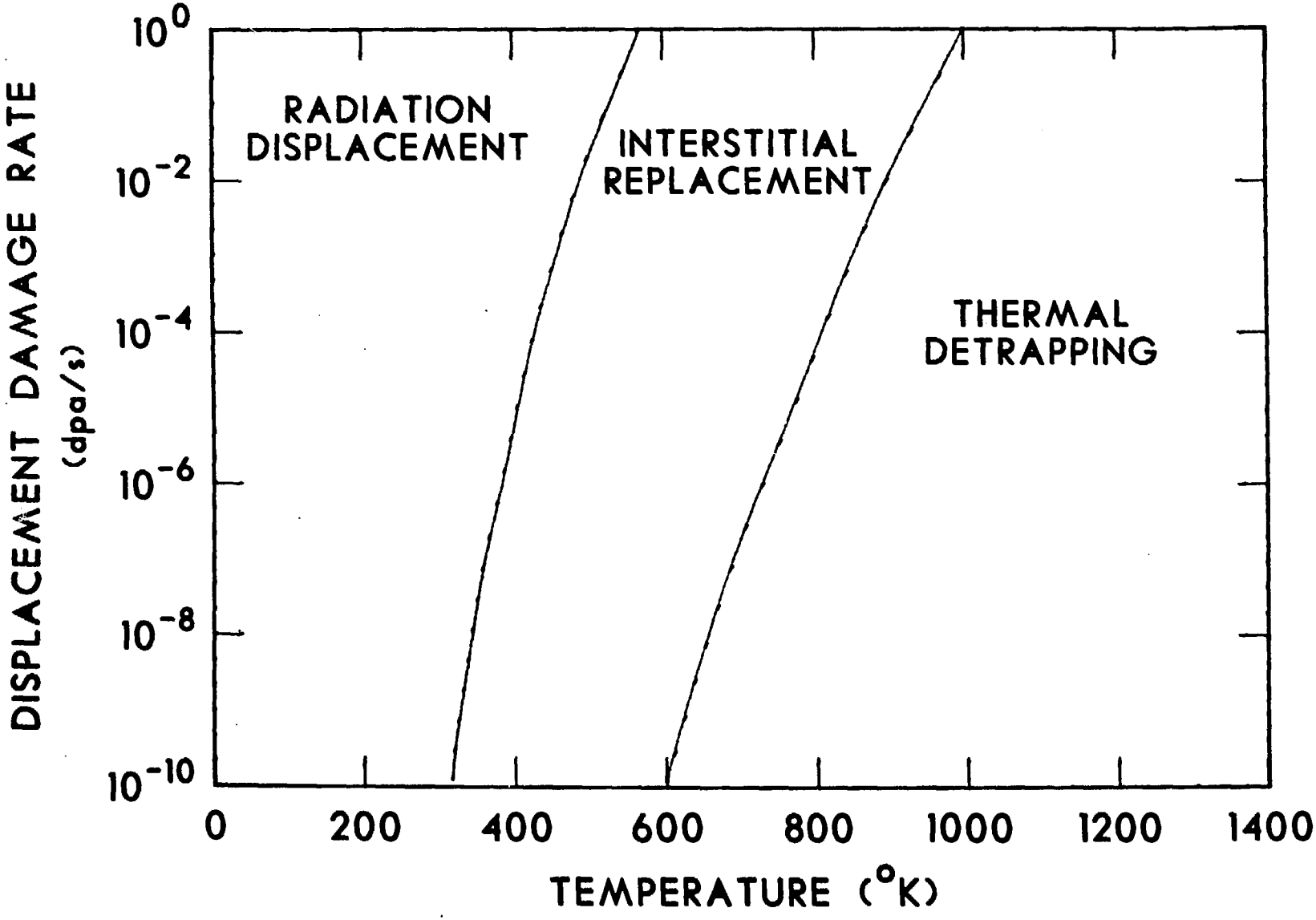

Fig 5, Mansur et al

ORNL-DWG 86C-10242

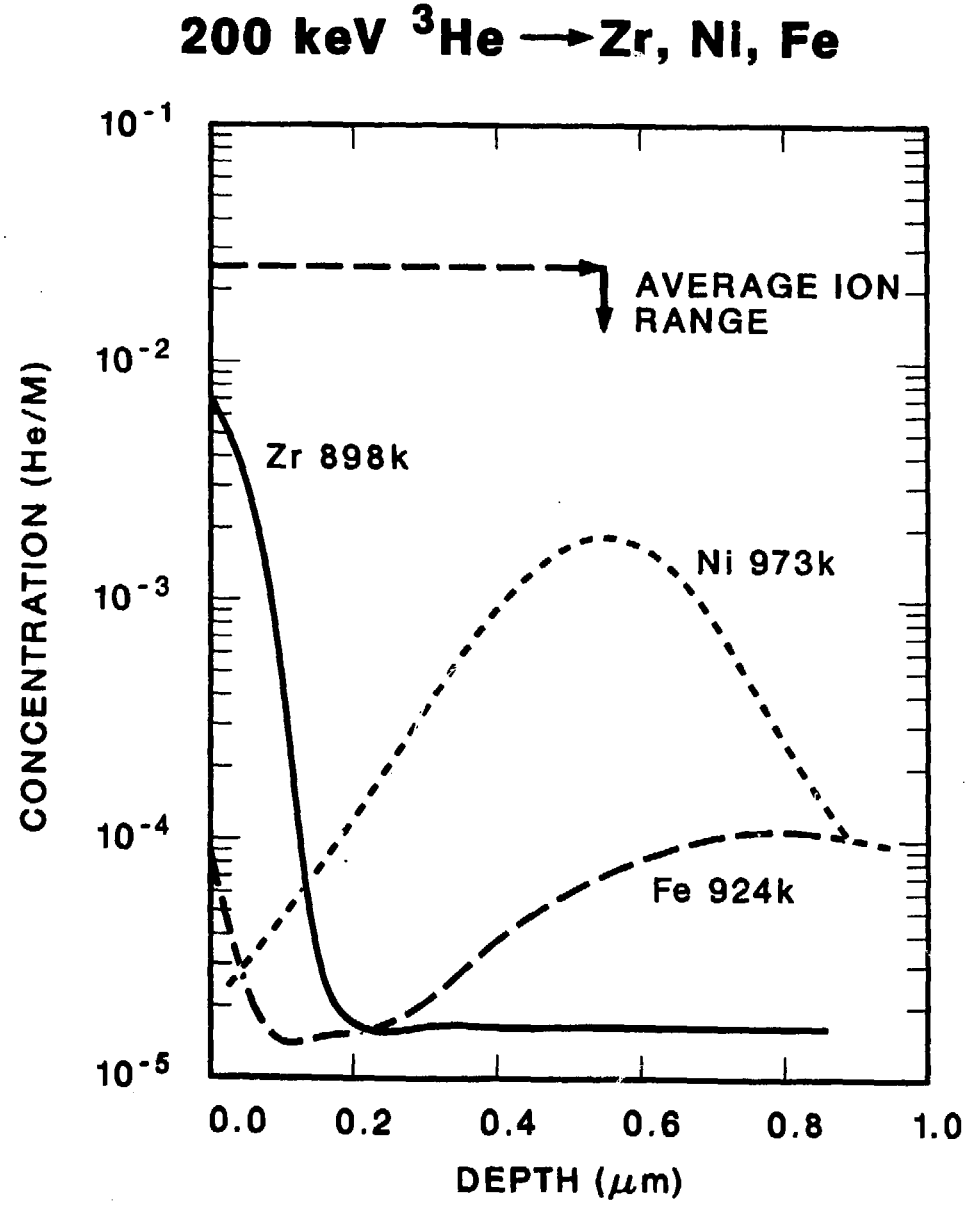

Fig 6. Mansur et al

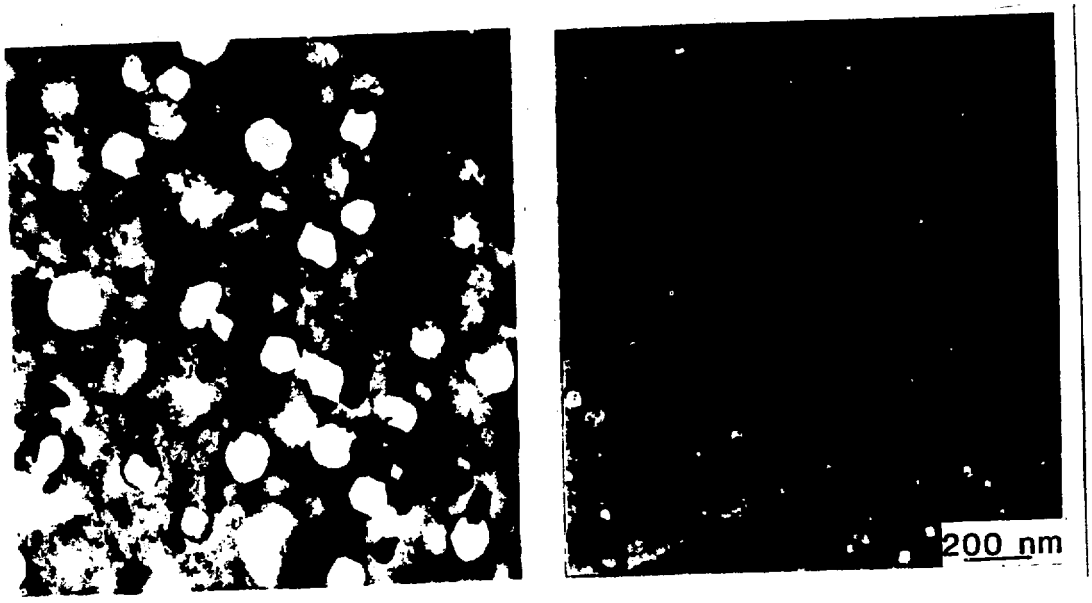

Fig 7, MANSUR et al.

THE EFFECT OF HELIUM ON PRECIPITATION IN NEUTRON IRRADIATED SA 316

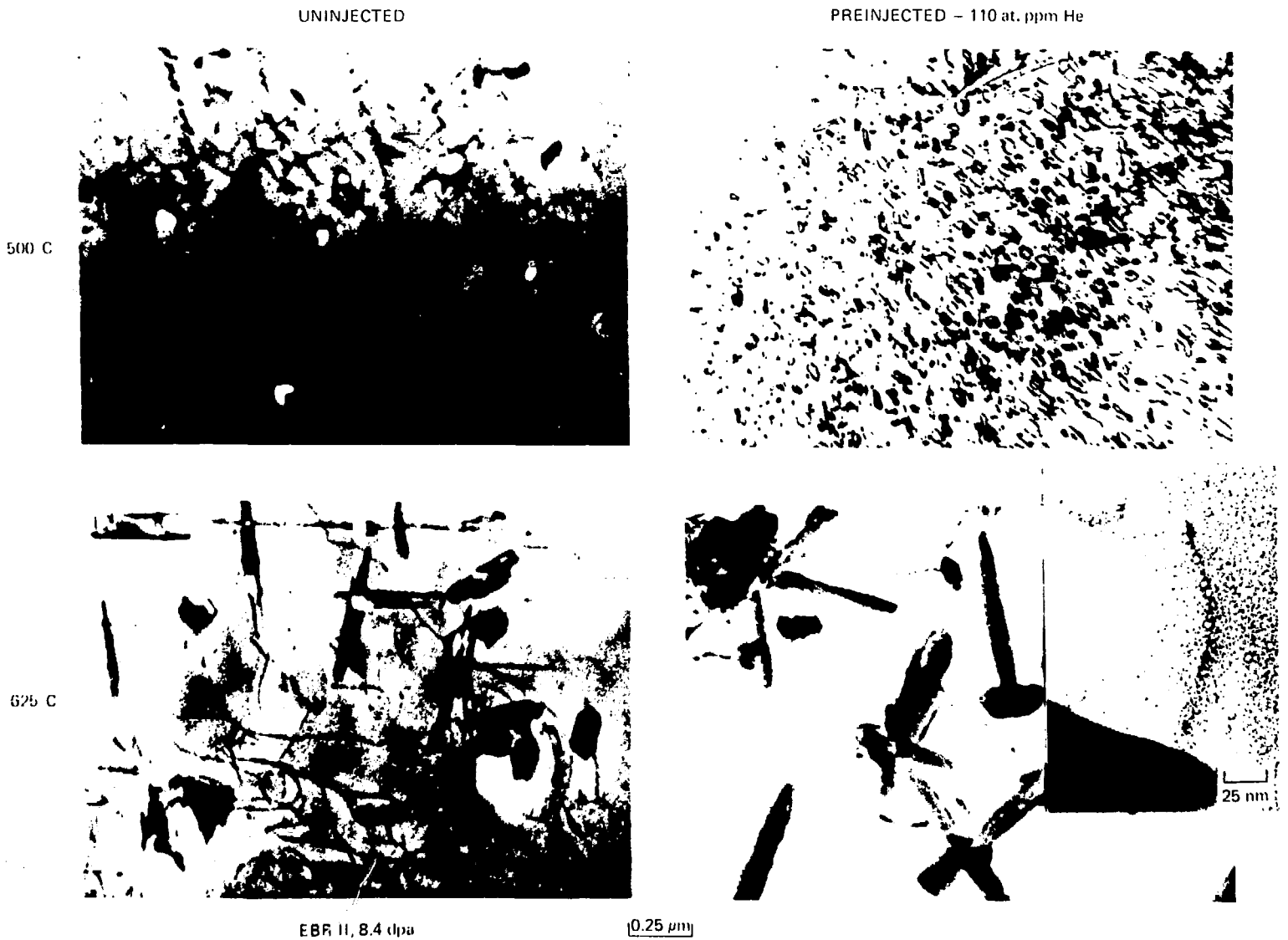

ornl

Fig 8, Mansur et al

ORNL-DWG 86C-9970

HELIUM AFFECTS PRECIPITATE VOLUME FRACTION AND TYPE IN IRRADIATED SA 316

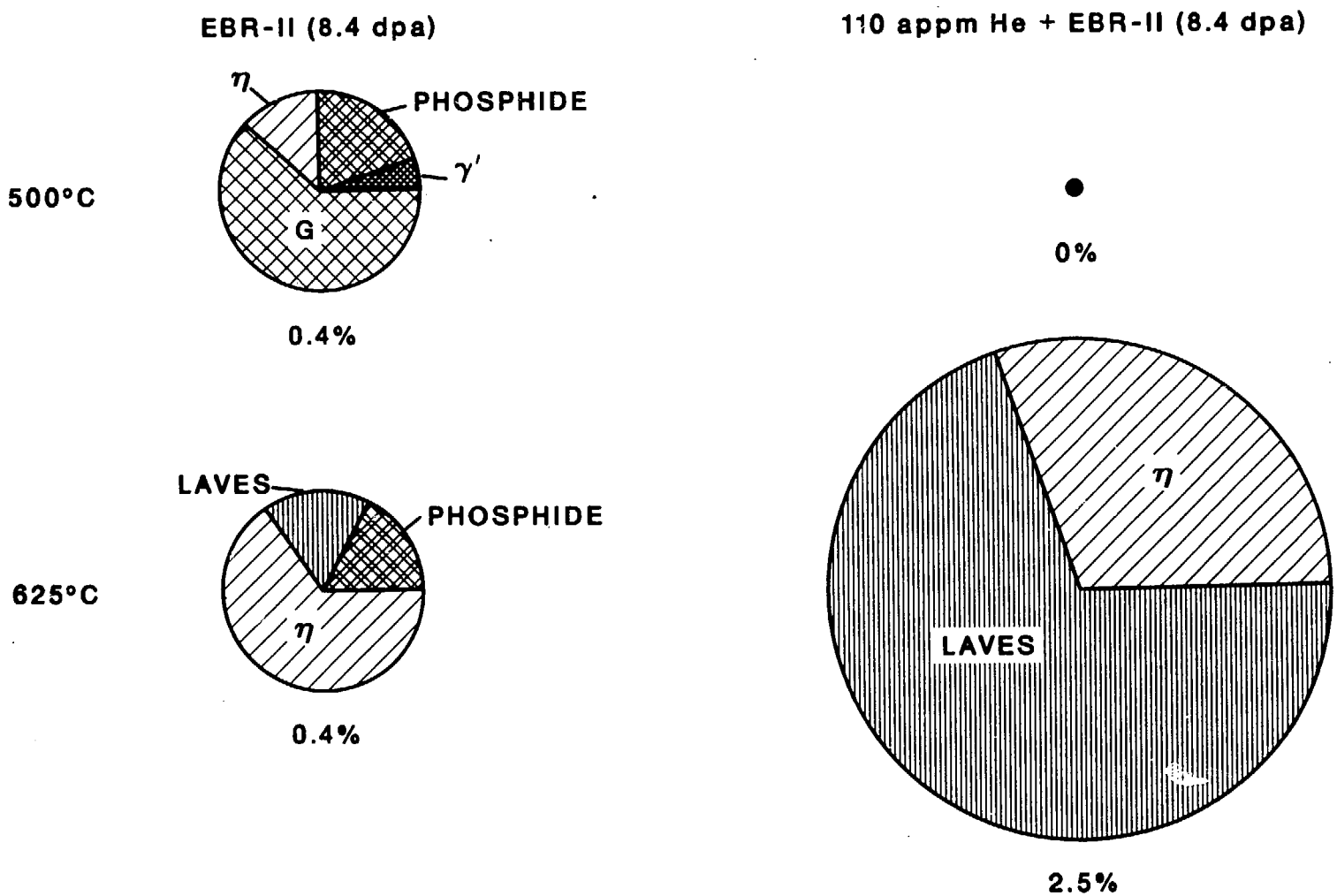

Fig 9 Mansur et al

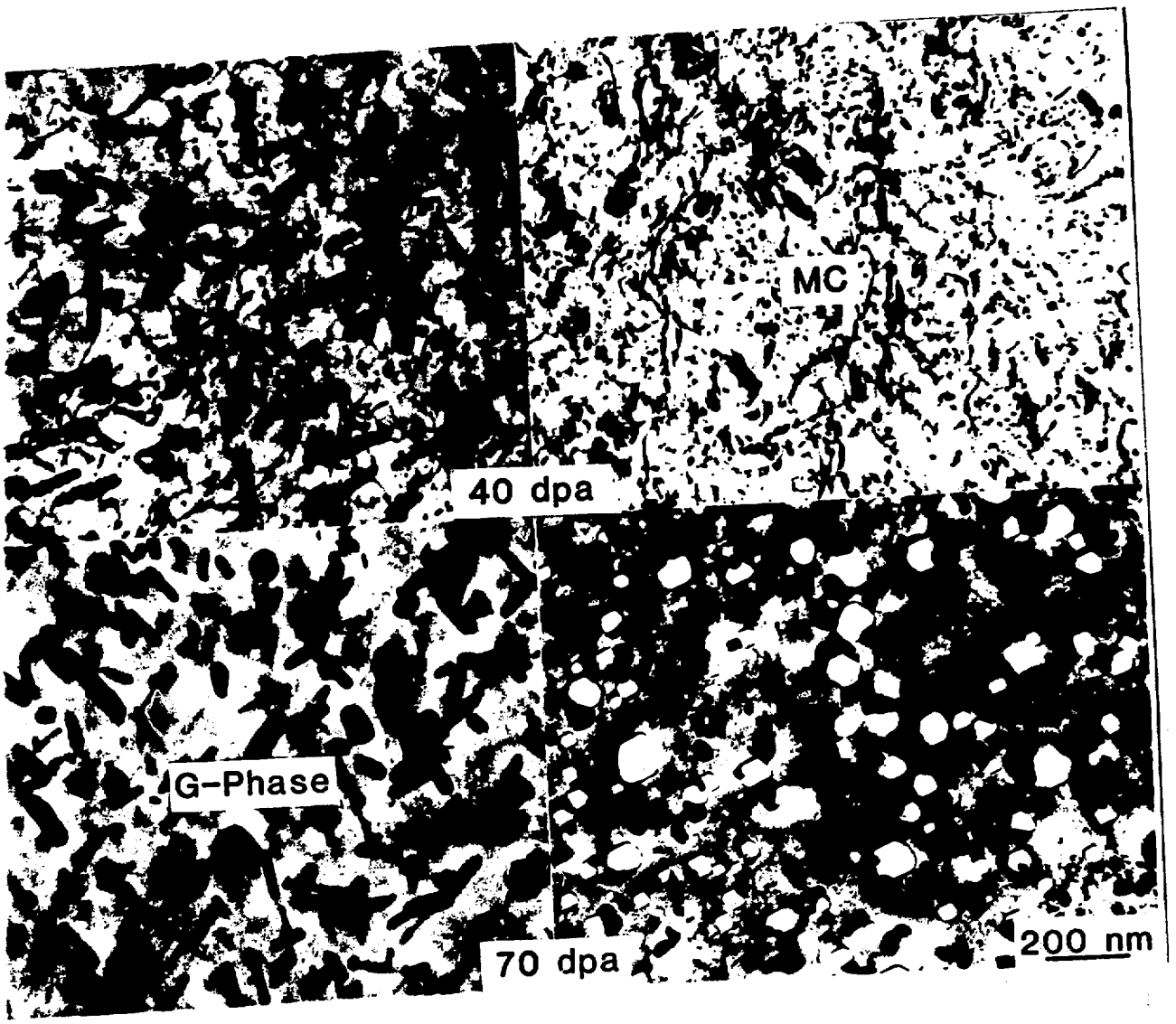

Fig. 10, Mansur et al.

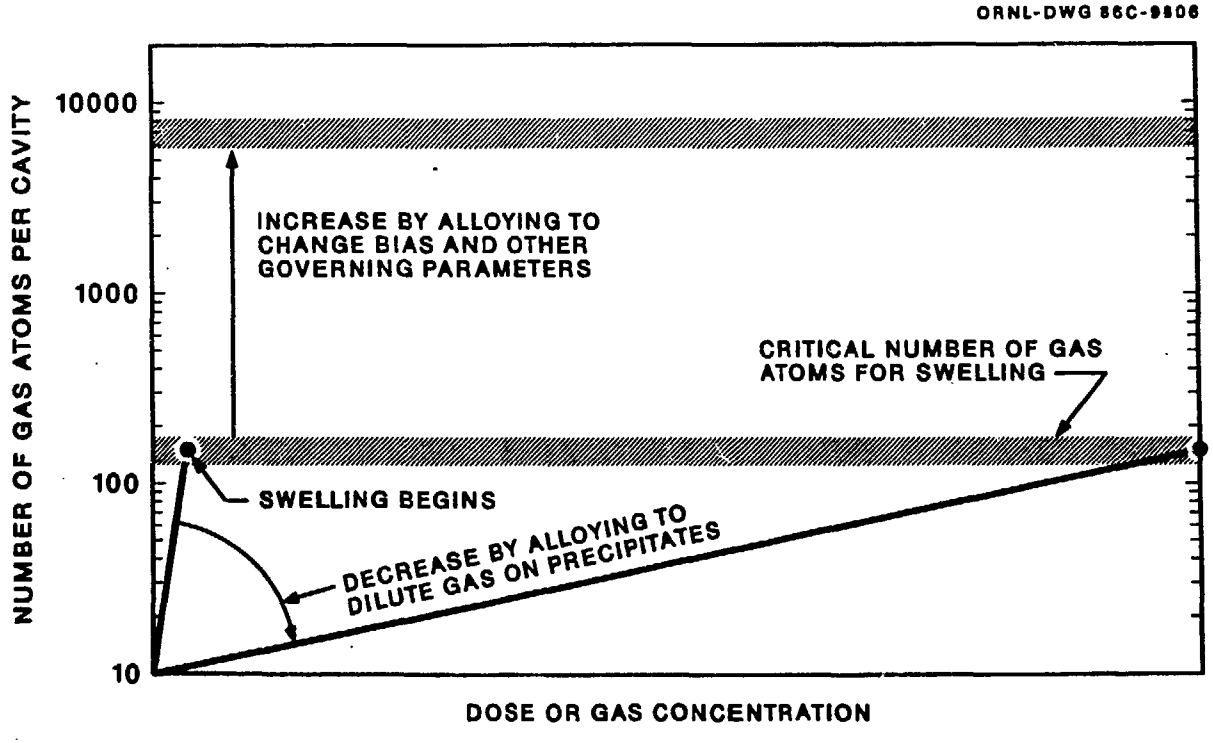

Fig 11, Mansur et al